Inorganic Chemistry

Article

pubs.acs.org/IC

Perturbation of the Charge Density between Two Bridged Mo_2 Centers: The Remote Substituent Effects

Tao Cheng, Miao Meng, Hao Lei, and Chun Y. Liu*

Department of Chemistry, Jinan University, 601 Huang-Pu Avenue West, Guangzhou 510632, China

Supporting Information

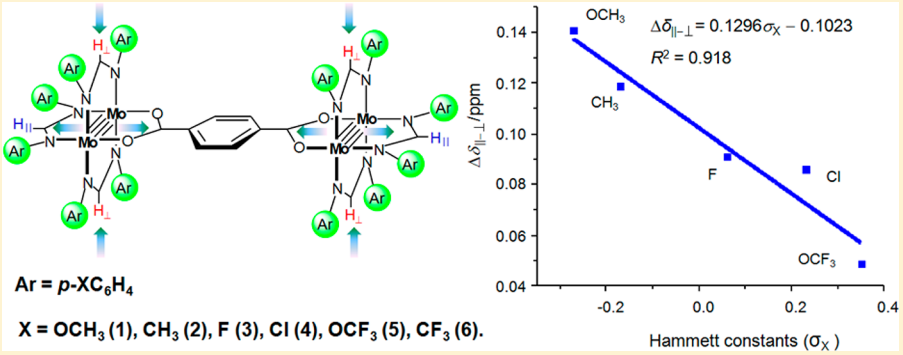

ABSTRACT: A series of terephthalate-bridged dimolybdenum dimers with various formamidinate ancillary ligands, denoted as $[Mo_2(ArNCHNAr)_3]_2(\mu\text{-}O_2CC_6H_4CO_2)$ (Ar = *p*-XC_6H_4, with X = OCH_3 (**1**), CH_3 (**2**), F (**3**), Cl (**4**), OCF_3 (**5**), and CF_3 (**6**)), has been synthesized and studied in terms of substituent effects on electron delocalization between the two dimetal sites. X-ray structural analyses show that these complexes share the same molecular scaffold with the *para*-substituents (X) being about 8 Å away from the Mo_2 center. It is found that the remote substituents have the capability to tune the electronic properties of the complexes. For the series **1** to **6**, the metal−metal bond distances (d_{Mo-Mo}) decrease slightly and continuously; the potential separations ($\Delta E_{1/2}$) for the two successive one-electron oxidations decrease constantly, and the metal to ligand transition energies (λ_{max}) increase in order. More interestingly, the two types of methine protons, $H_{\parallel}$ on the horizontal and $H_{\perp}$ on the vertical ligands with respect to the plane defined by the Mo−Mo bond vectors and bridging ligand, display separate resonant signals $\delta_{\parallel}$ and $\delta_{\perp}$ in the NMR spectra. The displacements of the chemical shifts, $\Delta\delta_{\parallel-\perp} = \delta_{\parallel} - \delta_{\perp}$, are getting smaller as the substituents vary from electron-donating to -withdrawing. These results show that the peripheral groups on the $[Mo_2]$ units function to fine-tune the metal−metal interactions crossing the bridging ligand. The experimental parameters, $\Delta E_{1/2}$, λ_{max}, and $\Delta\delta_{\parallel-\perp}$, which are linearly related with the Hammett constants (σ_X) of the X groups, can be used to probe the charge density on the two $[Mo_2]$ units and the electronic delocalization between them.

INTRODUCTION

Theoretical frameworks concerning the electron transfer (ET) kinetics and mechanism have been established based on the classical two-state model.[1,2] Experimentally, many molecular systems containing an electron donor (D) and an acceptor (A) separated by a bridge (B) have been studied to verify and refine the theories.[3,4] Generally speaking, electron-donating ability of the donor (or electron-withdrawing ability of the acceptor) and electron-transporting ability of the bridge are the two major factors that control the ET reaction and affect the mechanism. Much work has been focused on the bridging-ligand-mediated electronic coupling and electron transfer by modifying the length, conformation, and conjugation of the bridge.[5−7] In order to adjust the donor and acceptor properties, a variety of metal ions and clusters, such as Ru, Os, Fe, Mo_2, W_2, Ru_2, and Ru_3, have been employed as the redox sites to construct complex D−B−A systems.[8−10] On the other hand, as is well-known, variation of the peripheral ligands on a metal unit may significantly modify the energy level of the metal-based orbital, the HOMO in general, consequently, tuning the redox potential[9a,11] and modulating the photophysical and photochemical properties.[12,13] Thus, in complex D−B−A systems, the ET dynamics and kinetics, even the mechanism, could be substantially influenced by substituent effects through the ancillary ligands. For example, in the Ru_3−Ru_3 systems, it is observed that the donor−acceptor coupling and the intervalence transition are affected by the peripheral ligands.[14] However, a systematic study of substituent effects on donor−acceptor properties is scarcely seen, and our knowledge in this regard is insufficient.

Recent work demonstrates that D−B−A systems having quadruply bonded dimetal units (e.g., Mo_2 and W_2) as the redox sites are preferable for evaluation of the electronic coupling between the donor and acceptor, because in these complexes the transferring electrons, i.e., the δ electrons, are

Received: June 5, 2014
Published: August 13, 2014

   dx.doi.org/10.1021/ic501313q | Inorg. Chem. 2014, 53, 9213−9221

well-defined and the electron transfer path built by the d(δ)−p(π) conjugation is well-understood.[15,16] An abundance of [Mo_2]−bridge−[Mo_2] compounds, typically with dicarboxylate bridging ligands, have been synthesized for the study of bridge-mediated electronic interaction.[9b,17,18] In contrast, less attention has been paid to the impact of the ancillary ligands. Ren's work has demonstrated that the redox potential for a paddlewheel dimolybdenum formamidinate complex $Mo_2(form)_4$ is very sensitive to the variation of the *para*-substituents on the ligands.[19] Thus, it is expected that the substituent effects would significantly alter the electron-donating (or -accepting) ability of the [Mo_2] units in [Mo_2]−bridge−[Mo_2] complexes, consequently influencing the electronic coupling.

Hereby, in the present work, a series of six terephthalate-bridged dimolybdenum dimers with different aryl formamidinate ligands (ArNCHNAr) encompassing the Mo_2^{4+}cations has been synthesized. These complexes share a common molecular scaffold as shown in Scheme 1, but are differentiated by the aryl groups (Ar = *p*-XC_6H_5) with varying substituents (X), OCH_3 (**1**), CH_3 (**2**), F (**3**), Cl (**4**), OCF_3 (**5**), and CF_3 (**6**). As shown in Scheme 2, the ligands were carefully selected so that the electronic properties of the X groups in **1**−**6** vary from electron-donating to -withdrawing and the Hammett constants (σ_X) change correspondingly.[20] Provided with this complete series, we were able to systematically evaluate the substituent effects on the electronic properties of the *dimers of dimers*. Analyses of the experimental results, including structural, electrochemical, spectroscopic, and NMR data, shed light on the aspects pertinent to electron density distribution and charge transfer within the molecule.

Scheme 1. Molecular Scaffold for Complexes 1−6

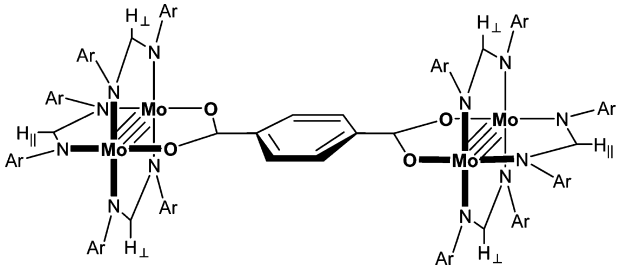

RESULTS AND DISCUSSION

Synthesis. To systematically tune the electronic property of the [Mo_2] units in the complexes, all the formamidinate ligands (ArNCHNAr) used for this study are equipped with two *para*-substituted phenyl groups (Scheme 2). The substituents were carefully chosen with their Hammett constants (σ_X) spanning from negative to positive so that the ligands possess the electronic properties varying from electron-donating to electron-withdrawing. The complex precursors $Mo_2(ArNCHNAr)_3(O_2CCH_3)$ (Ar = *p*-XC_6H_4 and X = OCH_3, CH_3, F, Cl, OCF_3, CF_3) were prepared by following the literature methods.[7b] In this work, the *dimers of dimers* **1**−**5** were synthesized by reactions of the corresponding precursor with terephthalic acid in the presence of a stoichiometric amount of sodium ethoxide, a different procedure from that used to first prepare compound **1**.[21]

$$2Mo_2(ArNCHNAr)_3(O_2CCH_3) + HO_2CC_6H_4CO_2H \xrightarrow[rt]{NaOC_2H_5/THF} [Mo_2(ArNCHNAr)_3]_2(\mu\text{-}O_2CC_6H_4CO_2)$$

However, we were unable to obtain **6** using a similar method, likely due to the scrambling reactions that yielded insoluble polymeric materials. This problem was overcome by self-assembling of the complex building blocks with tetraethylammonium terephthalate in C_2H_5OH/CH_2Cl_2 solution, which gave orange-red needle crystals.

Structural Results. The newly synthesized compounds (**2**−**6**) are structurally characterized by single-crystal X-ray diffraction. The crystallographic data are presented in Table 1. Compounds **2** and **6** crystallized in the monoclinic $P2_1/n$

Scheme 2. Formamidinate Ligands Used for the Preparation of 1−6

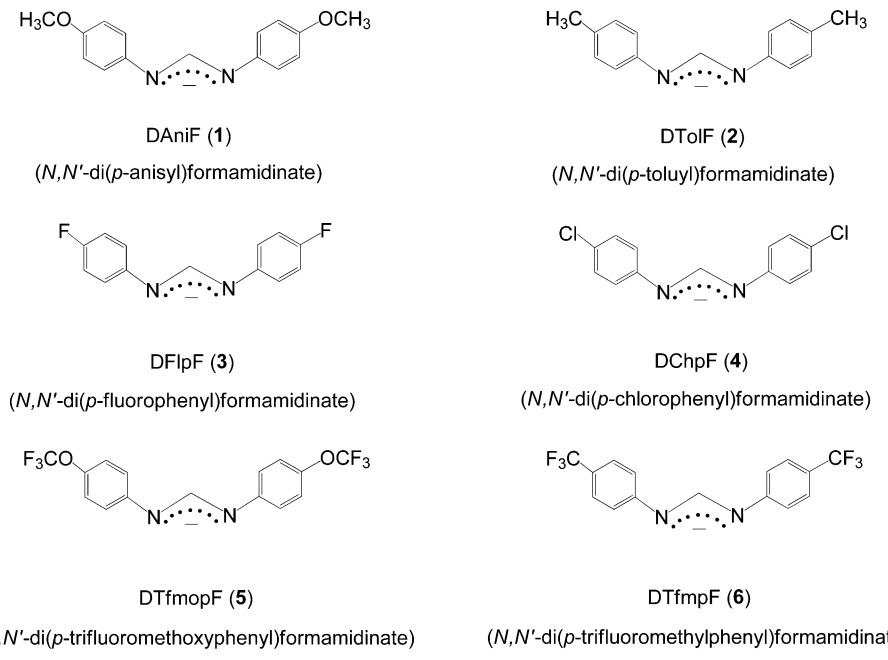

dx.doi.org/10.1021/ic501313q | Inorg. Chem. 2014, 53, 9213−9221

Table 1. Crystallographic Data for 2−6

	2·3.6CH_2Cl_2	**3**·2CH_2Cl_2	**4**·4C_4H_8O·2C_2H_6O	**5**·2CH_2Cl_2	**6**·2CH_2Cl_2
empirical formula	$C_{101.6}H_{101.2}Cl_{7.2}Mo_4N_{12}O_4$	$C_{88}H_{62}Cl_4F_{12}Mo_4N_{12}O_4$	$C_{106}H_{102}Cl_{12}Mo_4N_{12}O_{10}$	$C_{100}H_{62}Cl_4F_{36}Mo_4N_{12}O_{16}$	$C_{100}H_{62}Cl_4F_{36}Mo_4N_{12}O_4$
fw	2193.39	2105.06	2513.21	2897.15	2705.15
space group	$P2_1/n$	$P\bar{1}$	$P\bar{1}$	$P\bar{1}$	$P2_1/n$
a (Å)	19.8825(3)	10.5077(4)	10.5213(4)	11.3663(4)	11.4198(2)
b (Å)	10.13800(10)	12.6380(5)	14.6564(6)	15.0539(5)	34.0885(4)
c (Å)	27.7832(3)	18.1730(8)	18.3112(8)	17.5080(7)	13.9385(2)
α (deg)	90.00	83.994(4)	74.212(4)	91.343(3)	90.00
β (deg)	95.8240(10)	79.780(4)	89.818(3)	107.039(3)	108.783(2)
γ (deg)	90.00	68.635(4)	79.755(4)	108.251(3)	90.00
V (Å^3)	5571.32(12)	2209.68(16)	2670.77(19)	2698.17(17)	5137.07(13)
Z	2	1	1	1	2
T (K)	153	255	173	100	173
d_{calcd} (g/cm^3)	1.419	1.704	1.535	1.783	1.749
μ (mm^{-1})	6.586	7.500	7.038	5.828	5.980
R_1[a]	0.0549	0.0429	0.0383	0.0759	0.0439
wR_2[b]	0.1507	0.1162	0.1088	0.1892	0.1124

[a] $R_1 = \sum||F_o| - |F_c||/\sum|F_o|$. [b] $wR_2 = [\sum[w(F_o^2 - F_c^2)^2]/\sum[w(F_o^2)^2]]^{1/2}$.

Table 2. Selected Bond Distances (Å) of 2−6, in Comparison with Those of 1[a]

	1	**2**	**3**	**4**	**5**	**6**
Mo(1)−Mo(2)	2.0904(7)	2.0891(5)	2.0876(5)	2.0875(4)	2.0848(9)	2.0860(5)
Mo(1)−N(1)	2.155(5)	2.149(4)	2.136(4)	2.150(3)	2.138(6)	2.157(4)
Mo(1)−N(3)	2.123(5)	2.122(4)	2.151(4)	2.139(3)	2.134(6)	2.145(4)
Mo(1)−N(5)	2.152(5)	2.156(4)	2.146(4)	2.143(3)	2.127(6)	2.147(4)
Mo(2)−N(2)	2.137(5)	2.151(4)	2.156(4)	2.152(3)	2.140(6)	2.152(4)
Mo(2)−N(4)	2.119(5)	2.125(4)	2.116(4)	2.168(3)	2.150(6)	2.127(4)
Mo(2)−N(6)	2.137(5)	2.140(4)	2.150(4)	2.161(3)	2.159(6)	2.158(4)
Mo(1)−O(1)	2.144(4)	2.136(3)	2.131(3)	2.122(2)	2.137(5)	2.132(3)
Mo(2)−O(2)	2.122(4)	2.132(3)	2.155(3)	2.131(2)	2.127(4)	2.132(3)
O(1)−C(4)	1.266(7)	1.283(6)	1.281(5)	1.276(4)	1.270(8)	1.271(5)
O(2)−C(4)	1.279(6)	1.264(6)	1.272(6)	1.269(4)	1.280(9)	1.272(5)
C(4)−C(5)	1.473(8)	1.476(7)	1.482(6)	1.489(5)	1.484(9)	1.480(6)
Mo_2···Mo_2	11.240	11.233	11.288	11.215	11.235	11.231

[a] Data cited from ref 21.

space group with $Z = 2$, and **3**, **4**, and **5** in the $P\bar{1}$ space group with $Z = 1$. Therefore, each of the crystal structures is symmetrically generated by a crystallographically independent moiety. The selected bond distances are presented in Table 2. As expected, all these compounds exhibit a molecular scaffold similar to that for the reported methoxy (OCH_3) analogues or **1** (Figure 1).[21] The compounds are structurally different from each other by the *para*-substituents on the formamidinate ligands, which are separated from the associated Mo_2 center by about 8 Å.

In the series, the Mo−Mo bond lengths fall in the range of 2.0904(7)−2.0848(9) Å, which are typical for Mo−Mo quadruple bonds supported by formamidinate ligands. Notably, the bond distances are generally shorter than those for the dimolybdenum monomers having the same supporting ligands.[19] For example, compound **1** (X = OCH_3) has a Mo−Mo bond of 2.0904(7) Å, shorter than 2.0964(5) Å for $Mo_2(DAniF)_4$. Paddle-wheel complex $Mo_2(DAniF)_4$ has eight electron-donating OCH_3 groups, and heavier electron density on the dimetal center is anticipated relative to the dimer of dimers (**1**). The difference in metal−metal bond distance between these two compounds implies that the increased charge density is accumulated on the antibonding δ^* orbital, which weakens the Mo−Mo bond. In contrast, electron-withdrawing groups would reduce the electron density of the δ^* orbital, consequently shortening the metal−metal bond. Consistently, the Mo−Mo bond distances in the series tend to decrease as the substituents (X) change from electron-donating to -withdrawing. For example, compound **5**, with strongly electron-withdrawing groups, has the shortest Mo−Mo bond, ca. 2.0848(9) Å. A possible alternative explanation is that electron-donating groups increase the electron density on the Mo_2 center and raise the energy of the δ orbital. This would enforce the mixing of the metal orbital with the terephthalate π^* orbtial, as a result, slightly elongating the metal−metal bond.

Redox Properties of Complexes 1−6. Unlike the others, compounds **4** and **6** have a low solubility in dichloromethane. To obtain comparable data for the series, the electrochemical measurements were performed in tetrahydrofuran (THF). In electrochemical conditions, compounds **1**−**6** are supposed to undergo two one-electron oxidations, which remove one electron from each of the Mo_2^{4+} units. Since the electronic interaction between the two redox sites is sufficiently weak, the two waves in electrochemical cyclic voltammograms (CVs) and differential pulse voltammograms (DPVs) are not resolved. The $\Delta E_{1/2}$ values for **1**−**6** cannot be directly measured by peak-to-peak separations from the CV or DPV plots. The data ($\Delta E_{1/2}$) shown in Table 3 were estimated from the measurements of

dx.doi.org/10.1021/ic501313q | Inorg. Chem. 2014, 53, 9213−9221

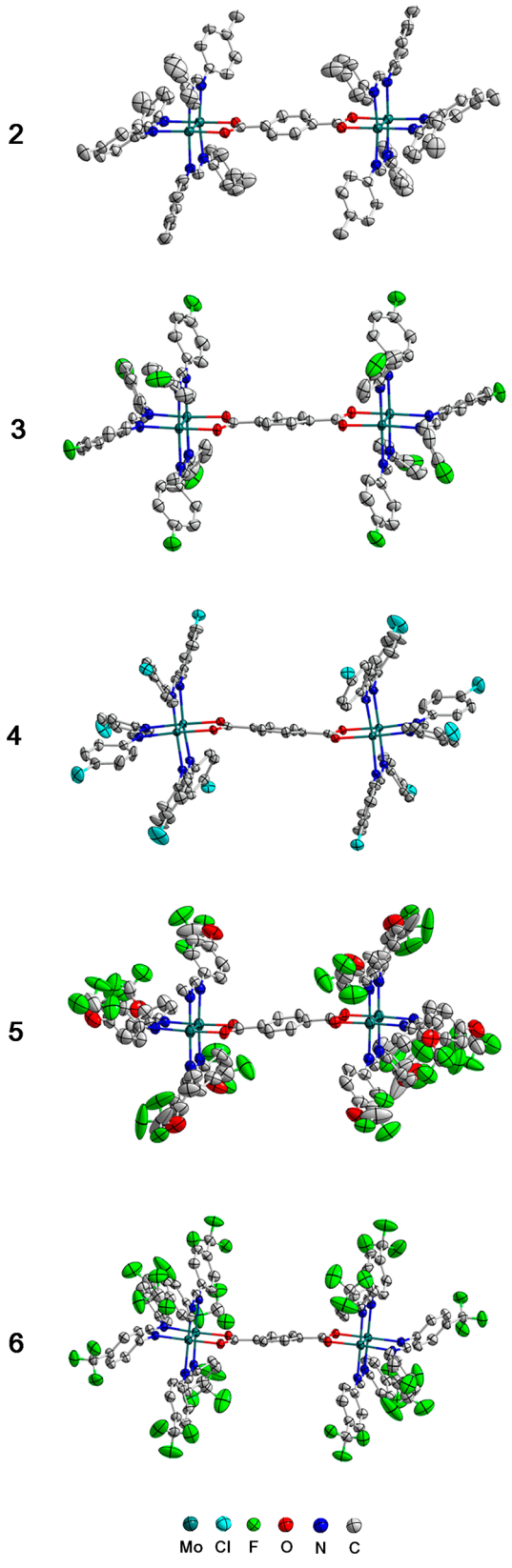

Figure 1. X-ray crystal structures for the terephthalate-bridged dimolybdenum dimers $[Mo_2(ArNCHNAr)_3]_2(\mu\text{-}O_2CC_6H_4CO_2)$ (Ar = p-XC_6H_4, with X = CH_3 (**2**), F (**3**), Cl (**4**), OCF_3 (**5**), and CF_3 (**6**)). Displacement ellipsoids are drawn at the 40% probability level. Hydrogen atoms are omitted for clarity.

Table 3. Electrochemical, Spectroscopic, and ^{1}H NMR Data for Complexes 1−6

parameter	1 (OCH_3)	2 (CH_3)	3 (F)	4 (Cl)	5 (OCF_3)	6 (CF_3)
σ_X	−0.27	−0.17	0.06	0.23	0.35	0.54
width (mV)[a]	166	159	135	125	116	107
$\Delta E_{1/2}$(mV)[b]	86	81	66	60	55	49
K_c	28	23	13	10	8	6
ΔG_c (cm^{-1})	−690	−650	−531	−477	−431	−371
λ_{max} (cm^{-1})	20 366	20 576	20 964	21 276	21 459	21 835
$\delta_{\parallel}$ (ppm)[c]	8.493	8.561	8.455	8.483	8.503	8.913
$\delta_{\perp}$ (ppm)	8.352	8.442	8.364	8.398	8.454	8.673
$\Delta\delta_{\parallel-\perp}$ (ppm)	0.141	0.119	0.091	0.085	0.049	0.240

[a]The widths at half-height ($i_{max}/2$) were measured from the DPV plots. [b]The $\Delta E_{1/2}$ values were estimated from the working curve (width vs $\Delta E_{1/2}$) in ref 22. [c]The ^{1}H NMR spectra for **1**−**5** were recorded in $CDCl_3$ and for **6** in DMSO-d_6.

DPV according to the Richardson−Taube methods.[22] For the complex series, the largest potential separation ($\Delta E_{1/2}$ = 86 mV) is found for **1**, with the most strongly electron-donating OCH_3 substituents, while compound **6** gives a $\Delta E_{1/2}$ value of 49 mV at the other extreme because of the most strongly electron-withdrawing effect of the CF_3 groups. As an intermediate species, compound **3**, equipped with F groups (σ_F = 0.06), has a $\Delta E_{1/2}$ value of 66 mV. It should be noted that the $\Delta E_{1/2}$ values measured in THF are smaller than the data obtained in dichloromethane because of the increased polarity of the solvent; for example, a $\Delta E_{1/2}$ of 91 mV was found for **1** in dichloromethane. Clearly, the remote X substituents impact not only the redox potential of the $[Mo_2]$ unit but also the potential separation, even though the X groups are symmetrically arranged on the molecular framework. The substituent effects on the electronic communication between the two $[Mo_2]$ units is best described by a linear relationship of the potential separation ($\Delta E_{1/2}$) versus the corresponding Hammett constant (σ_X); that is, $\Delta E_{1/2} = -47\sigma_X + 73$, as shown in Figure 2. The excellent fitting of data gives a correlation coefficient (R^2) of 0.973. A similar linear correlation between $\Delta E_{1/2}$ and σ_X was also observed in ferrocenyl monomers[23] and dimers.[24]

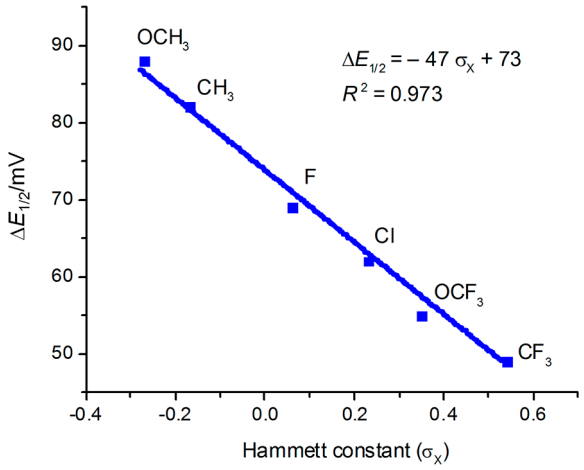

Figure 2. Plot of potential separations ($\Delta E_{1/2}$) versus Hammett constants of the substituents (σ_X). Linear fitting of the data gives a correlation coefficient (R^2) of 0.973, plotted using data from Table 3.

dx.doi.org/10.1021/ic501313q | Inorg. Chem. 2014, 53, 9213−9221

For the dimeric metal complexes, the potential separation ($\Delta E_{1/2}$) for the two one-electron redox processes corresponds to the free energy change (ΔG_c) for the comproportionation reaction and, thus, measures the thermodynamic stability of the mixed-valence species.[25] It is recognized that there are several factors that influence the magnitude of ΔG_c, for example, ΔG_s (statistical), ΔG_i (inductive), ΔG_e (electrostatic), and ΔG_r (resonance).[5a,26] Of the four terms, the last two contribute to enhance the electronic communication, but only the last term reflects the extent of electron delocalization. Therefore, the magnitude of $\Delta E_{1/2}$ can be utilized to weigh the strength of electronic communication only under certain circumstances in which the differences for the first two factors are negligible. Given the similar [Mo_2] building blocks and $Mo_2\cdots Mo_2$ separations, the potential separations ($\Delta E_{1/2}$) in this work are applicable for evaluation of the electronic delocalization between the two [Mo_2] sites. The $\Delta E_{1/2}-\sigma_X$ plot illustrates that electron-donating substituents enhance the electronic interaction and prompt electron delocalization.

Electronic Spectroscopy. All six compounds (**1**−**6**) display an intense charge transfer absorption band in the visible area, and the band energies (λ_{max}) vary in the range of 20366−21835 cm^{-1} (491−457 nm) (Table 3). The strong electron-donating ability of the methoxy groups (OCH_3) renders **1** the lowest electronic transition energy, while compound **6**, having strong electron-withdrawing substituents (CF_3), displays a high-energy absorption band. This influence of ligand substituents on the charge transfer energy is similar to the observation in other metal complex systems.[12] Remarkably, for this series, the charge transfer energies (λ_{max}, cm^{-1}) are also correlated to the Hammett constants of the substituents (σ_X) by a linear relationship, $\lambda_{max} = 1771\sigma_X + 20\,859$, as shown in Figure 3.

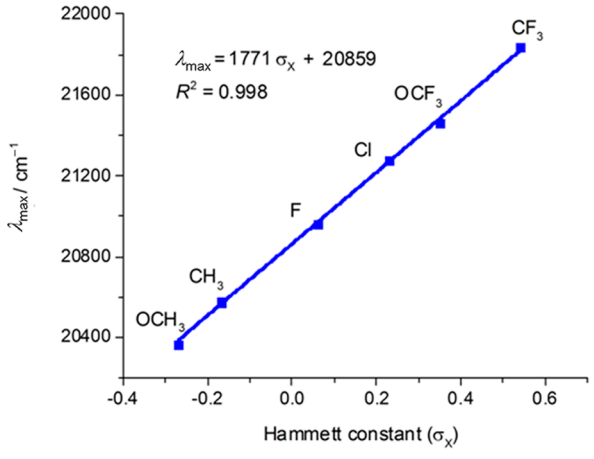

Figure 3. Plot of the metal-to-ligand transition energies (λ_{max}) versus the Hammett constants of the substituents (σ_X), plotted using data from Table 3. Linear fitting of the data gives a correlation coefficient (R^2) of 0.998.

In previous work on a series of closely related dimolybdenum dimers, the absorption bands in the visible region are assigned to the metal-to-ligand charge transfer (MLCT).[27] Calculations at the DFT level indicate that the HOMO of the complexes is a metal-based orbital resulting from the out-of-phase ($\delta-\delta$) combination of the δ orbitals with a filled π orbital of the bridging ligand, while the LUMO is a bridging-ligand-based orbital obtained by the interaction of an empty π^* orbital with the in-phase metal orbitals ($\delta+\delta$). The HOMO → LUMO transition gives rise to the intense MLCT absorption. Thus, the relatively low energy of the MLCT band for **1** implies its small HOMO−LUMO energy gap. Obviously, the electron-donating groups, e.g., OCH_3, are capable of raising the δ orbital energy and lowering the energy gap. In contrast, the high-energy MLCT band for **6** is due to the electron-withdrawing property of the CF_3 substituents. Therefore, these results indicate that fine-tuning the HOMO−LUMO energy gap can be realized by selective introduction of the peripheral substituents. In the previous section, we have seen that electron-donating groups build up electron density on the Mo_2 center. Here, the spectroscopic results show that the electron-donating groups increase the metal−ligand orbital mixing and facilitate the charge transfer. Therefore, the spectral results support the variation of Mo−Mo bond length in the series. Furthermore, the observed substituent effects on the electronic ML transition energy are similar to the spectroscopic behaviors reported for organic conjugated systems, in which the spectral absorbance is red-shifted by the electron-donating substituents.[28] This similarity confirms that the charge transfer platform (CTP) of the complexes, established by the d(δ)−p(π) orbital conjugation, involves the two quadruply bonded Mo_2 units and the bridging ligand.

Optical analyses for D−B−A systems may give rise to the electronic coupling matrix element (H) that quantitatively measures the donor−acceptor coupling strength.[29] According to superexchange formalism,[30] a strategy to enhance the metal-to-metal electronic coupling is to lower the metal-to-ligand (ML) and ligand-to-metal (LM) transition gaps. Our recent work on the related systems shows that the MLCT energy for the mixed-valence species is essentially equal to that for the corresponding neutral precursor.[31] Therefore, it is expected that in the mixed-valence systems corresponding to this series the remote peripheral groups would function in modulating the electronic coupling effect and dominating the electron transfer process. For instance, the electron transfer in mixed-valence complex $\mathbf{1}^+$ should be relatively faster than that in $\mathbf{6}^+$. In a neutral D−B−A system, on the other hand, the electron-donating groups on the metal coordination units are expected to facilitate the charge separation and stabilize the two degenerate excited states, D^+-B^--A and $D-B^--A^+$.[32]

^{1}H NMR Spectra. Given the molecular scaffold as shown in Scheme 1, each of the complexes (**1**−**6**) has six formamidinate ligands (ArNCHNAr) in two sets, two horizontal and four vertical with respect to the [Mo_2]−bridge−[Mo_2] platform. With a D_{2h} symmetry in common, the molecules show two ^{1}H NMR signals in a ratio of 1:2 for the two types of methine protons, namely, $H_\parallel$ on the horizontal ligands and $H_\perp$ on the vertical ones. It is also important to note that while the $H_\parallel$'s resonate at the downfield side (with a larger $\delta_\parallel$), the $H_\perp$'s exhibit the signal at the upfield side (with a smaller $\delta_\perp$), for example, $\delta_\parallel$ 8.493 ppm and $\delta_\perp$ 8.352 ppm for **1**. More interestingly, as shown in Figure 4 and Table 3, the displacement of the chemical shifts for $H_\parallel$ and $H_\perp$, $\Delta\delta_{\parallel-\perp} = \delta_\parallel - \delta_\perp$, vary by compound, implying a substituent dependence of the $\Delta\delta$ values. The largest chemical displacement is observed for **1** ($\Delta\delta_{\parallel-\perp}$ = 0.141 ppm), and the smallest $\Delta\delta_{\parallel-\perp}$ (0.049 ppm) for **5**. It is remarkable that by changing the remote X groups from electron-donating to -withdrawing, the $\Delta\delta_{\parallel-\perp}$ values for **1**−**5** decrease continuously. Unfortunately, compound **6**, which has the most strongly electron-withdrawing substituents (CF_3), has a poor solubility in deuterated

dx.doi.org/10.1021/ic501313q | Inorg. Chem. 2014, 53, 9213−9221

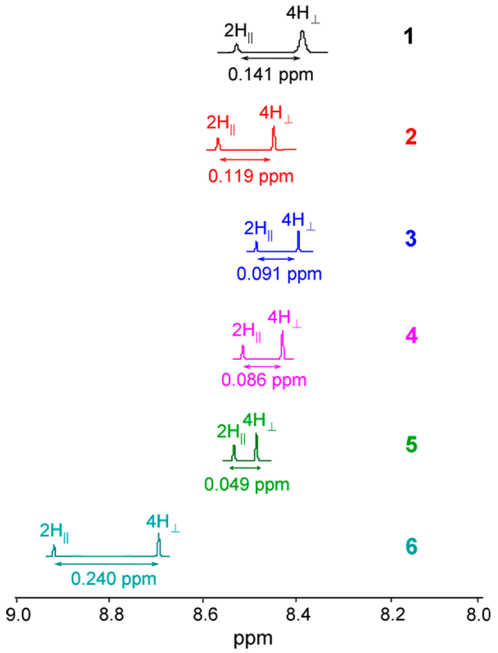

Figure 4. Partial ^{1}H NMR spectra for complexes **1**–**6**, presented to show the resonances of the methine protons (ArNC*H*NAr) in two orthogonal positions. The spectra for **1**–**5** were measured in deuterated chloroform ($CDCl_3$) and for **6** in deuterated dimethyl sulfoxide (CD_3SOCD_3).

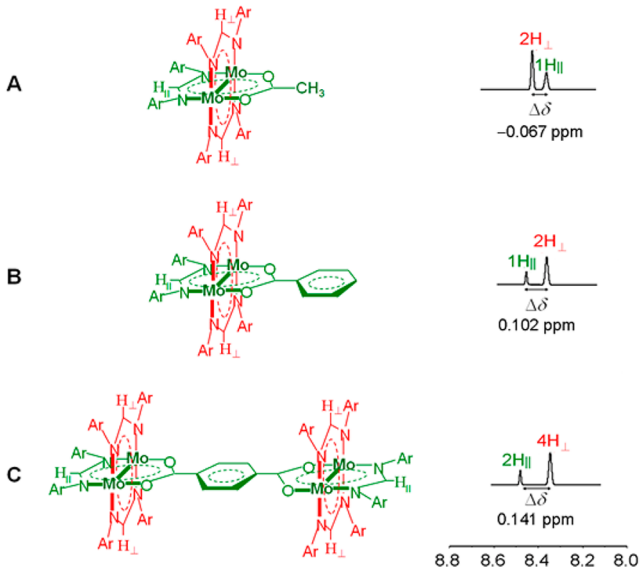

Figure 5. Schematics of aryl formamidinate supported dimolybdenum monomers and dimer accompanied by the corresponding ^{1}H NMR resonances for the methine protons in two orthogonal positions ($H_\parallel$ and $H_\perp$): (A) for $Mo_2(DAniF)_3(O_2CCH_3)$; (B) for $Mo_2(DAniF)_3(O_2CC_6H_5)$; and (C) for $[Mo_2(DAniF)_3]_2(\mu$-$O_2CC_6H_4CO_2)$.

chloroform ($CDCl_3$) and the spectrum was measured in deuterated dimethyl sulfoxide (CD_3SOCD_3). Thus, the $\Delta\delta_{\parallel-\perp}$ value of 0.240 ppm is not comparable with those for the other compounds.

To understand the displacement of chemical shifts ($\Delta\delta_{\parallel-\perp}$) for the two sets of methine protons, we may start with a dimolybdenum monomer. Paddlewheel complexes $Mo_2(form)_4$ generally show a singlet of magnetic resonance in the downfield region because of the diamagnetic anisotropy of the Mo–Mo quadruple bond.[19] When one of the formamidinate ligands is replaced by an acetate anion, the pseudo D_{4h} symmetry is destroyed, and the resultant mixed-ligand compound $Mo_2(form)_3(O_2CCH_3)$ presents two singlets in a ratio of 1:2 for the methine protons on the *trans* and *cis* formamidinate ligands. For example, the spectrum for $Mo_2(DAniF)_3(O_2CCH_3)$ shows the resonant signals $\delta_\parallel$ at 8.386 ppm and $\delta_\perp$ at 8.453 ppm,[7b] which gives a negative $\Delta\delta_{\parallel-\perp}$value (−0.067 ppm) (Figure 5). Interestingly, for the benzoate derivative $Mo_2(DAniF)_3(O_2CC_6H_5)$, the $H_\parallel$'s present the NMR signal downfield relative to the $H_\perp$'s. The chemical shifts $\delta_\parallel$ and $\delta_\perp$ are separated by $\Delta\delta_{\parallel-\perp}$ = 0.102 ppm (Figure 5).[31a] The two compounds have the same coordination shell and similar electronic configurations for the Mo_2 cores. The only difference is that the methyl group in the former is replaced by a phenyl group in the latter. Obviously, the aromatic phenyl group is responsive for the $\delta_\parallel$ and $\delta_\perp$ shifts toward the opposite directions. Therefore, our explanation for this phenomenon is that in $Mo_2(DAniF)_3(O_2CC_6H_5)$ the electron density on the dimetal center is extended to the phenyl ring through d(δ)–p(π) conjugation, which enlarges the horizontal aromatic system. According to the ring current model,[33] it is understandable that the coplanar $H_\parallel$'s would experience a deshielding effect induced by the multinuclei π system and the $H_\perp$s, on the other hands, are located in the shielding zone of the induced magnetic field. Therefore, the shifts of $\delta_\parallel$ and $\delta_\perp$ are indicative of the increased charge density on the horizontal plane containing two Mo–Mo bonds and a phenyl ring, that is, the CTP as defined.

Compared to $Mo_2(DAniF)_3(O_2CC_6H_5)$, the dimeric $[Mo_2(DAniF)_3]_2(\mu$-$O_2CC_6H_4CO_2)$, or **1**, shows similar chemical shifts $\delta_\parallel$ and $\delta_\perp$, but the $\Delta\delta_{\parallel-\perp}$ value is increased to 0.141 ppm (Figure 5). Apparently, the increased $\Delta\delta_{\parallel-\perp}$ value for **1** is due to the further enlarged conjugated system containing two $[Mo_2]$ units across the phenylene group. More importantly, the results show that in the series the chemical shifts $\delta_\parallel$ and $\delta_\perp$ as well as the displacement $\Delta\delta_{\parallel-\perp}$ are dependent upon the electronic property of the substituent X, as indicated by Figure 4. A linear relationship between $\Delta\delta_{\parallel-\perp}$ and the Hammett constants (σ_X), $\Delta\delta_{\parallel-\perp} = -0.1296\sigma_X + 0.1023$, is found for complexes **1**–**5** with a correlation coefficient (R^2) of 0.918 (Figure 6). It is noticed that the magnitude of $\Delta\delta_{\parallel-\perp}$ for **4** with Cl substituents is larger than expected from the linear

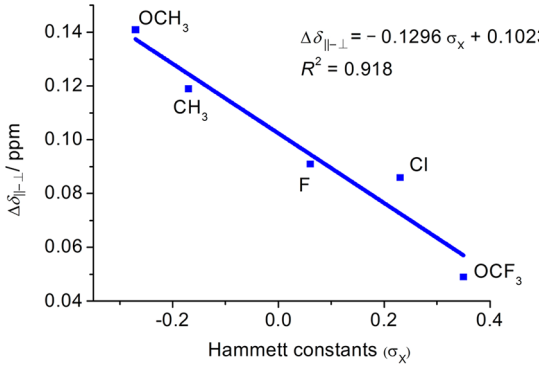

Figure 6. Plot of displacements of the chemical shifts ($\Delta\delta_{\parallel-\perp}$) versus the Hammett constants of the substituents (σ_X), plotted using data from Table 3. Linear fitting of the data gives a correlation coefficient (R^2) of 0.918.

dx.doi.org/10.1021/ic501313q | *Inorg. Chem.* 2014, 53, 9213–9221

relationship. This result is compatible with the observation obtained in other systems,[34] showing that the Cl substituent behaves somehow as an electron-donating group. In previous work on chalcogen-bridged dimolybdenum clusters $[Mo_2(DAniF)_3]_2(\mu\text{-}E)_2$ (E = O, S, Se), we found that the large $\Delta\delta_{\|-\perp}$value is attributed to the strong aromaticity for the six-membered core $[Mo_2E_2Mo_2]$.[35] Similarly, in the current system, a greater magnitude of $\Delta\delta_{\|-\perp}$ is a reflection of the better d(δ)−p(π) conjugation. Furthermore, the protons on the central phenyl group also exhibit variable NMR signals corresponding to the remote substituents. With electron-donating X groups ($\sigma_X < 0$), the three compounds (**1**, **2**, and **3**) present chemical shifts smaller than those for compounds **4** and **5** ($\sigma_X > 0$), for example, 8.349 ppm for **1** (X = OCH_3) and 8.432 ppm for **5** (X = OCF_3). Therefore, it is evidenced that the X groups with $\sigma_X < 0$ increase the electron density on the bridge, or *vice versa*, although they are located far away from the central phenylene group. These results conform well to the variation of the Mo−Mo bond distances and the electronic spectra, showing the substituent effects on electron density on the CT platform. On this basis, the magnitude of $\Delta\delta_{\|-\perp}$ can be utilized as a probe to assess electron delocalization between the two Mo_2 centers.

On the contrary, Ren's work on paddle-wheel molecules indicated that the magnetic anisotropy surrounding the Mo−Mo quadruple bond was unrelated to the Hammett constants of the *para*-substituents on the ligands.[19] Presumably, in that case, the D_{4h} symmetry of the molecules causes the electron-donating or -withdrawing effects of the substituents to be offset. When the Mo_2 unit is equipped with an aromatic ligand, as shown by $Mo_2(DAniF)_3(O_2CC_6H_5)$, charge transfer from the dimetal center to the ligand is feasible via the d(δ)−p(π) conjugation; as a result, the charge density on the two orthogonal chelating planes is unbalanced. For the *dimers of dimers*, owing to the δ orbital that is symmetry related to the ligand π orbtials in two perpendicular directions, the charge on the vertical chelating ring is able to be transferred "right-angularly" to the CT platform.

CONCLUSIONS

In summary, we have synthesized and characterized a series of six dimolybdenum dimers (**1**−**6**), in which the quadruply bonded Mo_2^{4+} units are supported by various aryl formamidinate ligands. The ancillary ligands are carefully chosen in order for the *para*-substituents (X) on the phenyl groups to vary from electron-donating to -withdrawing with the Hammett constants (σ_X) ranging from −0.27 (OCH_3) to 0.54 (CF_3). Given the same molecular scaffold for the series, substituent effects on the electronic properties for the complex series have been studied systematically by means of X-ray diffraction, electrochemistry, and electronic and NMR spectroscopies. It is found that the substituents located far away from the dimetal centers (ca. 8 Å) prompt significant perturbation of the electron density on the molecules, consequently affecting the electronic coupling and charge distribution between the two $[Mo_2]$ sites. The electron-donating groups slightly lengthen the Mo−Mo quadruple bond, indicating that the extra electron density is accumulated on the δ^* orbital. Remarkably, the experimental parameters, the redox potential separation ($\Delta E_{1/2}$), and the MLCT energy (λ_{max}) are found to be directly and linearly correlated to the Hammett constants (σ_X) of the substituents. It is interesting to find that the methine protons on the vertical ($H_\perp$) and horizontal ($H_\|$) formamidinate ligands resonate at different chemical shifts, $\delta_\perp$ and $\delta_\|$, respectively. The displacement between $\delta_\|$ and $\delta_\perp$, namely, $\Delta\delta_{\|-\perp}$, also shows the substituent dependence, thus being an efficient probe for the electron density on the charge transfer platform. Our study demonstrates that in D−B−A complexes the peripheral substituents on the redox sites modify the charge distribution and fine-tune the electronic communication between the two bridged dimetal centers.

EXPERIMENTAL SECTION

Materials and Methods. All manipulations were performed in a nitrogen-filled glovebox or by using standard Schlenk-line techniques. All solvents were purified using a Vacuum Atmospheres solvent purification system or freshly distilled over appropriate drying agents under nitrogen. Starting materials formamidines (ArNCHNHAr)[36] and the dimolybdenum precursors $Mo_2(ArNCHNAr)_3(O_2CCH_3)$[7b] were synthesized according to published methods and characterized by ^{1}H NMR spectra.

Physical Measurements. Elemental analyses were determined using an Elementar Vario EL elemental analyzer. UV−visible spectra were measured on a Shimadzu UV-3600 UV−vis−NIR spectrophotometer. Cyclic voltammograms were performed using a CH Instruments model CHI660D electrochemical analyzer in a 0.10 M THF solution of ^{n}Bu$_4$NPF$_6$ with Pt working and auxiliary electrodes, a Ag/AgCl reference electrode, and a scan rate of 100 mV/s^{-1}. All potentials are referenced to the Ag/AgCl electrode. ^{1}H NMR spectra were recorded on a Bruker-500 spectrometer.

X-ray Structure Determinations. For compounds **2**, **3**, and **5**, single crystals for X-ray structure determinations were obtained by diffusion of ethanol into the corresponding dichloromethane solution and for **4** by diffusion of ethanol into its tetrahydrofuran solution. Single-crystal data for **2** and **3** were collected on an Agilent Gemini S Ultra diffractometer with Cu Kα radiation (λ = 1.541 78 Å), and those for **4**, **5**, and **6** were collected on an Agilent Xcalibur Nova diffractometer with Cu Kα radiation (λ = 1.541 78 Å). The empirical absorption corrections were applied using spherical harmonics, implemented in the SCALE3 ABSPACK scaling algorithm.[37] All the structures were solved using direct methods, which yielded the positions of all non-hydrogen atoms. Hydrogen atoms were placed in calculated positions in the final structure refinement. Structure determination and refinement were carried out using the SHELXS-97 and SHELXL-97 programs, respectively.[38] All non-hydrogen atoms were refined with anisotropic displacement parameters.

General Procedure for Preparation of 2, 3, 4, and 5. A solution of sodium ethoxide (0.20 mmol) in 10 mL of ethanol was transferred to a solution of $Mo_2(ArNCHNAr)_3(O_2CCH_3)$ (0.20 mmol) in 20 mL of THF. After stirring at room temperature for 2 h, the solvent were removed under vacuum. The residue was dissolved using 25 mL of CH_2Cl_2 and filtered off through a Celite-packed funnel. The filtrate was mixed with terephthalic acid (0.1 mmol). The mixture was stirred for 3 h, producing a bright red, microcrystalline solid. The product was collected by filtration and washed with ethanol (3 × 20 mL).

Yield of **2**: 0.136 g, 72%. ^{1}H NMR δ (ppm in $CDCl_3$): 8.561 (s, 2H, −NC*H*N−), 8.442 (s, 4H, −NC*H*N−), 8.316 (s, 4H, aromatic C−*H*), 6.868(d, 16H, aromatic C−*H*), 6.503 (d, 16H, aromatic C−*H*), 6.709 (d, 8H, aromatic C−*H*), 6.223 (d, 8H, aromatic C−*H*), 2.231 (s, 24H, −C*H*$_3$), 2.176 (s, 12H, −C*H*$_3$). UV−vis, λ_{max} nm (ε, M^{-1} cm^{-1}): 486 (1.5 × 10^4). Anal. Calcd for $C_{98}H_{94}Mo_4N_{12}O_4$: C, 62.36; H, 5.02; N, 8.90. Found: C, 63.11; H, 4.89; N, 8.94.

Yield of **3**: 0.126 g, 68%. ^{1}H NMR δ (ppm in $CDCl_3$): 8.455 (s, 2H, −NC*H*N−), 8.364 (s, 4H, −NC*H*N−), 8.421 (s, 4H, aromatic C−*H*), 6.827(m, 16H, aromatic C−*H*), 6.614 (m, 16H, aromatic C−*H*), 6.597 (m, 8H, aromatic C−*H*), 6.205 (m, 8H, aromatic C−*H*). UV−vis, λ_{max} nm (ε, M^{-1} cm^{-1}): 477 (1.4 × 10^4). Anal. Calcd for $C_{86}H_{58}Mo_4N_{12}O_4F_{12}$: C, 53.38; H, 3.02; N, 8.69. Found: C, 53.77; H, 3.10; N, 8.77.

Yield of **4**: 0.155 g, 75%. ^{1}H NMR δ (ppm in $CDCl_3$): 8.483 (s, 2H, −NC*H*N−), 8.398 (s, 4H, −NC*H*N−), 8.385 (s, 4*H*, aromatic C−*H*), 7.107 (d, 16H, aromatic C−*H*), 6.553 (d, 16H, aromatic C−*H*), 6.903

dx.doi.org/10.1021/ic501313q | Inorg. Chem. 2014, 53, 9213−9221

(d, 8H, aromatic C−*H*), 6.171 (d, 8H, aromatic C−*H*). UV−vis, λ_{max} nm (ε, M^{-1} cm^{-1}): 470 (1.4×10^4). Anal. Calcd for $C_{86}H_{58}Mo_4N_{12}O_4Cl_{12}$: C, 48.43; H, 2.74; N, 7.88. Found: C, 47.67; H, 2.81; N, 7.97.

Yield of **5**: 0.193 g, 73%. ^{1}HNMR δ (ppm in $CDCl_3$): 8.503 (s, 2H, −NC*H*N−), 8.454 (s, 4H, −NC*H*N−), 8.432 (s, 4H, aromatic C−*H*), 7.011 (d, 16H, aromatic C−*H*), 6.652 (d, 16H, aromatic C−*H*), 6.747 (d, 8H, aromatic C−*H*), 6.187 (d, 8H, aromatic C−*H*), 3.742. UV−vis, λ_{max} nm (ε, M^{-1} cm^{-1}): 466 (1.4×10^4). Anal. Calcd for $C_{98}H_{58}F_{36}Mo_4N_{12}O_{16}$: C, 43.16; H, 2.14; N, 6.16. Found: C, 44.67; H, 2.27; N, 6.20.

Preparation of 6. A solution of $Mo_2(DTfmpF)_3(O_2CCH_3)$ (0.062 g, 0.05 mmol) in 10 mL of CH_2Cl_2 was added to a 50 mL Schlenk tube, and then a solution of tetraethylammonium terephthalate (0.0106 g, 0.025 mmol) in 40 mL of ethanol was added carefully. After several days orange-red needle crystals formed and were collected directly. Yield: 0.047 g, 75%. ^{1}H NMR δ (ppm in CD_3SOCD_3): 8.913 (s, 2H, −NC*H*N−), 8.673 (s, 4H, −NC*H*N−), 8.460 (s, 4H, aromatic C−*H*), 7.470 (d, 16H, aromatic C−*H*), 6.906 (d, 16H, aromatic C−*H*), 7.196 (d, 8H, aromatic C−*H*), 6.643 (d, 8H, aromatic C−*H*). UV−vis, λ_{max} nm (ε, M^{-1} cm^{-1}): 457 (1.3×10^4). Anal. Calcd for $C_{98}H_{58}F_{36}Mo_4N_{12}O_4$: C, 46.43; H, 2.31; N, 6.63. Found: C, 46.67; H, 2.50; N, 6.74.

■ ASSOCIATED CONTENT

Ⓢ Supporting Information

^{1}H NMR spectra and selected bond distances. This material is available free of charge via the Internet at http://pubs.acs.org.

■ AUTHOR INFORMATION

Corresponding Author

*E-mail (C. Y. Liu): tcyliu@jnu.edu.cn.

Notes

The authors declare no competing financial interest.

■ ACKNOWLEDGMENTS

We thank the National Natural Science Foundation of China (Nos. 20871093, 90922010, and 21371074) and Jinan University for financial support.

■ REFERENCES

(1) (a) Marcus, R. A. *J. Chem. Phys.* **1956**, *24*, 966−978. (b) Marcus, R. A. *Rev. Mod. Phys.* **1993**, *65*, 599−610.

(2) (a) Hush, N. S. *Prog. Inorg. Chem.* **1967**, *8*, 391−444. (b) Hush, N. S. *Electrochim. Acta* **1968**, *13*, 1005−1023.

(3) (a) Creutz, C.; Taube, H. *J. Am. Chem. Soc.* **1969**, *91*, 3988−3989. (b) Creutz, C.; Taube, H. *J. Am. Chem. Soc.* **1973**, *95*, 1086−1094. (c) Creutz, C. *Prog. Inorg. Chem.* **1983**, *30*, 1−73.

(4) (a) Piepho, S. B.; Krausz, E. R.; Schatz, P. N. *J. Am. Chem. Soc.* **1978**, *100*, 2996−3005. (b) Piepho, S. B. *J. Am. Chem. Soc.* **1988**, *110*, 6319−6326. (c) Piepho, S. B. *J. Am. Chem. Soc.* **1990**, *112*, 4197−4206.

(5) (a) Crutchley, R. J. *Adv. Inorg. Chem.* **1994**, *41*, 273−325. (b) Launay, J.-P. *Chem. Soc. Rev.* **2001**, *30*, 386−397.

(6) (a) Eng, M. P.; Albinsson, B. *Angew. Chem., Int. Ed.* **2006**, *45*, 5626−5629. (b) Albinsson, B.; Eng, M. P.; Pettersson, K.; Winters, M. U. *Phys. Chem. Chem. Phys.* **2007**, *9*, 5847−5864.

(7) (a) Aguirre-Etcheverry, P.; O'Hare, D. *Chem. Rev.* **2010**, *110*, 4839−4864. (b) Cotton, F. A.; Liu, C. Y.; Murillo, C. A.; Villagrán, D.; Wang, X. *J. Am. Chem. Soc.* **2003**, *125*, 13564−13575.

(8) (a) Goldsby, K. A.; Meyer, T. J. *Inorg. Chem.* **1984**, *23*, 3002−3010. (b) Demadis, K. D.; Hartshorn, C. M.; Meyer, T. J. *Chem. Rev.* **2001**, *101*, 2655−2685.

(9) (a) Ren, T. *Chem. Rev.* **2008**, *108*, 4185−4207. (b) Chisholm, M. H. *Coord. Chem. Rev.* **2013**, *257*, 1576−1583.

(10) (a) Ito, T.; Hamaguchi, T.; Nagino, H.; Yamaguchi, T.; Washington, J.; Kubiak, C. P. *Science* **1997**, *277*, 660−663. (b) Lear, B. J.; Glover, S. D.; Salsman, J. C.; Londergan, C. H.; Kubiak, C. P. *J. Am. Chem. Soc.* **2007**, *129*, 12772−12779.

(11) (a) Chen, P.; Finikova, O. S.; Ou, Z. P.; Vinogradov, S. A.; Kadish, K. M. *Inorg. Chem.* **2012**, *51*, 6200−6210. (b) Gansäuer, A.; Kube, C.; Daasbjerg, K.; Sure, R.; Grimme, S.; Fianu, G. D.; Sadasivam, D. V.; Flowers, R. A. *J. Am. Chem. Soc.* **2014**, *136*, 1663−1671.

(12) Goldberg, P. K.; Pundsack, T. J.; Splan, K. E. *J. Phys. Chem. A* **2011**, *115*, 10452−10460.

(13) (a) LeCours, S. M.; Guan, H. W.; DiMagno, S. G.; Wang, C. H.; Therien, M. J. *J. Am. Chem. Soc.* **1996**, *118*, 1497−1503. (b) Priyadarshy, S.; Therien, M. J.; Beratan, D. N. *J. Am. Chem. Soc.* **1996**, *118*, 1504−1510.

(14) (a) Ito, T.; Hamaguchi, T.; Nagino, H.; Yamaguchi, T.; Kido, H.; Zavarine, I. S.; Richmond, T.; Washington, J.; Kubiak, C. P. *J. Am. Chem. Soc.* **1999**, *121*, 4625−4632. (b) Londergan, C. H.; Salsman, J. C.; Ronco, S.; Kubiak, C. P. *Inorg. Chem.* **2003**, *42*, 926−928.

(15) Cotton, F. A.; Murillo, C. A.; Walton, R. A. *Multiple Bonds between Metal Atoms*, 3rd ed.; Springer: New York, 2005.

(16) Burdzinski, G. T.; Chisholm, M. H.; Chou, P.-T.; Chou, Y.-H.; Feil, F.; Gallucci, J. C.; Ghosh, Y.; Gustafson, T. L.; Ho, M.-L.; Liu, Y.; Ramnauth, R.; Turro, C. *Proc. Natl. Acad. Sci. U.S.A.* **2008**, *105*, 15247−15252.

(17) (a) Cotton, F. A.; Donahue, J. P.; Lin, C.; Murillo, C. A. *Inorg. Chem.* **2001**, *40*, 1234−1244. (b) Cotton, F. A.; Donahue, J. P.; Murillo, C. A. *J. Am. Chem. Soc.* **2003**, *125*, 5436−5450.

(18) Chisholm, M. H.; Patmore, N. J. *Acc. Chem. Res.* **2007**, *40*, 19−27.

(19) (a) Lin, C.; Protasiewicz, J. D.; Smith, E. T.; Ren, T. *J. Chem. Soc., Chem. Commun.* **1995**, *22*, 2257−2258. (b) Lin, C.; Protasiewicz, J. D.; Smith, E. T.; Ren, T. *Inorg. Chem.* **1996**, *35*, 6422−6428.

(20) (a) Hammett, L. P. *Physical Organic Chemistry*; McGraw-Hill: New York, 1970. (b) Shorter, J. *Correlation Analysis in Organic Chemistry*; Clarendon Press: Oxford, 1973. (c) Hansch, C.; Leo, A.; Taft, R. W. *Chem. Rev.* **1991**, *97*, 165−195.

(21) Cotton, F. A.; Donahue, J. P.; Lin, C.; Murillo, C. A.; Rockwell, J. *Acta Crystallogr.* **2002**, *E58*, m298−m300.

(22) Richardson, D. E.; Taube, H. *Inorg. Chem.* **1981**, *20*, 1278−1285.

(23) Bobula, T.; Hudlický, J.; Novák, P.; Gyepes, R.; Císařová, I.; Štěpnička, P.; Kotora, M. *Eur. J. Inorg. Chem.* **2008**, 3911−3920.

(24) (a) Hildebrandt, A.; Lang, H. *Dalton Trans.* **2011**, *40*, 11831−11837. (b) Hildebrandt, A.; Lang, H. *Organometallics* **2013**, *32*, 5640−5653.

(25) Richardson, D.; Taube, H. *Coord. Chem. Rev.* **1984**, *60*, 107−129.

(26) Evans, C. E. B.; Naklicki, M. L.; Rezvani, A. R.; White, C. A.; Kondratiev, V. V.; Crutchley, R. J. *J. Am. Chem. Soc.* **1998**, *120*, 13096−13103.

(27) Xiao, X.; Liu, C. Y.; He, Q.; Han, M. J.; Meng, M.; Lei, H.; Lu, X. *Inorg. Chem.* **2013**, *52*, 12624−12633.

(28) Cao, C. Z.; Zhu, Y.; Chen, G. F. *J. Phys. Org. Chem.* **2013**, *26*, 834−839.

(29) (a) Hush, N. S. *Prog. Inorg. Chem.* **1967**, *8*, 391−444. (b) Hush, N. S. *Electrochim. Acta* **1968**, *13*, 1005−1023.

(30) Creutz, C.; Newton, M. D.; Sutin, N. *J. Photochem. Photobiol. A: Chem.* **1994**, *82*, 47−59.

(31) (a) Liu, C. Y.; Xiao, X.; Meng, M.; Zhang, Y.; Han, M. J. *J. Phys. Chem. C* **2013**, *117*, 19859−19865. (b) Xiao, X.; Meng, M.; Lei, H.; Liu, C. Y. *J. Phys. Chem. C* **2014**, *118*, 8308−8315.

(32) Chisholm, M. H.; Lear, B. J.; Moscatelli, A.; Peteanu, L. A. *Inorg. Chem.* **2010**, *49*, 3706−3713.

(33) (a) Pople, J. A. *J. Chem. Phys.* **1956**, *24*, 1111−1112. (b) Johnson, C.; E. Bovey, F. A. *J. Chem. Phys.* **1958**, *29*, 1012−1014.

(34) Valverde-Aguilar, G.; Wang, X. H.; Plummer, E.; Lockard, J. V.; Zink, J. I.; Luo, Y.; Weaver, M. N.; Nelsen, S. F. *J. Phys. Chem. A* **2008**, *112*, 7332−7341.

(35) (a) Fang, W.; He, Q.; Tan, Z. F.; Liu, C. Y.; Lu, X.; Murillo, C. A. *Chem.—Eur. J.* **2011**, *17*, 10288−10296. (b) Tan, Z. F.; Liu, C. Y.; Li, Z.; Meng, M.; Weng, N. S. *Inorg. Chem.* **2012**, *51*, 2212−2221.
(36) Shriner, R. L.; Neumann, F. W. *Chem. Rev.* **1944**, *35*, 351−425.
(37) *CrysAlis RED*, Version 1.171.31.7; Oxford Diffraction Ltd, 2006.
(38) Sheldrick, G. M. *SHELXTL*, Version 6.12; Bruker Analytical X-ray Systems, Inc.: Madison, WI, 2000.